JOURNAL OF METEOROLOGY AND CLIMATE SCIENCE
J. Met & Clim. Sci. 21(1): 29-53 (June, 2022)

Land cover Accuracy Assessment in Okitipupa, Ondo State, Nigeria; Application of Atmospheric correction and Machine learning Algorithms.

O. J. Aigbokhan*, C. S. Ofordu, N. E. Essien, N. C. Mba.

Department of Environmental Modelling and Biometrics, Forestry Research Institute of Nigeria.
[*Corresponding Author: E-mail: oseyomon255@gmail.com]

ABSTRACT

The interaction of solar radiation with the atmosphere causes changes in the solar radiation that the Earth's surface reflects satellite sensors. Therefore, by eliminating air influences from satellite images, applying an atmospheric correction aid in determining genuine surface reflectance values and retrieving physical properties of the Earth's surface, including surface reflectance. Perhaps the most crucial step in pre-processing data from satellites that have been remotely detected is atmospheric correction. Here, we assessed Okitipupa, Ondo State, Nigeria's land cover classification using Landsat 8 image. The acquired Landsat image was subjected to Quick Atmospheric Correction (QUAC), Dark Object Subtraction (DOS), and Fast Line-of-sight Atmospheric Analysis of Spectral Hypercubes (FLAASH) algorithm. The corrected image was applied to create the land cover classification using random forest (RF) and support vector machine (SVM) techniques. Four different classes were used in this study: built-up, shrubs, vegetation, and wetland/river. The land cover classification accuracy was in the following order: 0.98 and 0.96 > 0.97 and 0.95 for SVM_FLAASH and SVM_QUAC. This was followed by SVM_QUAC with an overall accuracy of 0.97 and a kappa coefficient of 0.95. Quick Atmospheric Correction (QUAC), Dark Object Subtraction (DOS), and Fast Line-of-Sight Atmospheric Analysis of Spectral Hypercubes are the three atmospheric correction algorithms (FLAASH).

Keywords: Accuracy assessment, Contrast ratio, Operational Land Imager, Pattern curve, Spectral Hypercubes,

Copyright © 2022 Nigerian Meteorological Society

INTRODUCTION

Natural ecosystems need to be monitored and assessed in order for environmental elements to be sustainable (He et al., 2005). Over the past few decades, environmental mapping has been fueled by conventional evaluation methods such as sizable field samples (Ruppert and Linstädter, 2014). Even if these methods are accurate, covering large tracts of land demands a lot of resources, including money and effort (Xie et al., 2009). In response to developments in remote sensing and geographic information systems, several studies on faster methods for atmospheric correction have been done (Zhao et al., 2016). Air pollutants may be detected by the spheric dispersion and absorption, which show considerable variations with time, space, and wavelength. In addition, surface reflectance is significantly influenced by the height of the terrain, with a larger effect in mountainous regions (Körner et al., 2008). In particular, when conducting multitemporal investigations (Vázquez-Quintero et al., 2016; Prieto-Amparán et al., 2016), this highlights the need for atmospheric correction to limit the impacts of noise present during the acquisition of satellite images (Pons et al., 2014). For example, the problem of data saturation is believed to have a substantial influence on the results when measuring the biomass of plants (Tan et al., 2012; Roy et al., 2016). The primary goal of atmospheric correction is to correct influences on satellite images through the assessment of optical qualities (Chrysoulakis et al., 2010). The Landsat satellite has provided data with complete worldwide coverage since 1972. (Cohen and Goward, 2004). This is an essential tool for monitoring environmental changes throughout the world (Hansen and Loveland, 2012). Due to the multiplicity of models and parameter choices, the main disadvantage of many atmospheric adjustments for different sensors is the difficulty to understand the data. The Harmonized Landsat and Sentinel-2 Project is one attempt to combine satellite data (Claverie et al., 2018). It intends to seamlessly transmit Sentinel-2 and Landsat 8 products. Model-based atmospheric corrections rely on radiative modelling with a specific focus on atmospheric optical characteristics at the time of picture capture, unlike image-based approaches, which rely on image metadata and statistical analysis of top of the atmosphere (TOA) reflectance. (Lantzanakis and coworkers, 2016) Various atmospheric and radiometric corrections were made to the images' raw data to transform them into reflectance values methods that have been developed (Chavez 1988; Kaufman et al.,1997; Janzen, et al., 2006). For instance, the MODTRAN accuracy model is used in

Copyright © 2022 Nigerian Meteorological Society

the Fast Line of Sight Atmospheric Analysis of Spectral Hypercubes (FLAASH) algorithm, created by Spectral Science Inc. (Burlington, MA, USA) (Kruse 2004), to determine the properties of the surface and atmosphere's reflectance and to explain how adjacency affects the atmosphere's dispersion. The brightness of the image and any potential cloud or fog effects are eliminated using the Atmospheric Correction for Flat Terrain 2 (ATCOR2) method to get the values of the terrestrial surface (User Manual, 2013). The Dark Object Subtract (DOS) method, which is based on the image's features, is the most often used method for recognizing changes in land usage (Paolini et al., 2006; Cui et al., 2014). Several studies have compared various techniques for reversing the effects of the atmosphere. El Hajj et al. (2008) compared a 6S method employing SPOT5 data and relative radiometric normalization in this regard. Calliceco and Dell'Acqua (2011) compared and contrasted the 6S and MODTRAN algorithms. The FLAASH and QUAC algorithms were studied by Agrawal et al. (2011) in their study. Nazeer et al. (2014) tested five atmospheric correction algorithms across the sand, turf, grass, and water surfaces: 6S, FLAASH, ATCOR, DOS, and ELM. Lopez-Serrano et al (2016) evaluated the efficacy of the COST, ATCOR2, FLAASH, 6S, and TOA algorithms for the assessment of forest above-ground biomass. Martins et al (2017) compared the 6S, ACOLYTE, and Sen2Cor methods employed with the brand-new Sentinel 2-MSI platform. Many classification algorithms have been created in recent years, especially in the machine learning sector. Certain machine learning approaches have been used for classification tasks for more than 10 years. Support vector machines (SVM) and random forests (RF) are two of the most often used methods (Koc-San, 2013; Adam et al., 2014; Ballanti et al., 2016; Sonobe et al., 2017). While Rumora et al. (2019) investigated the impact of atmospheric changes on spectral reflectance values, Vanonckelen et al. (2013) and Lin et al. (2015) offered instances of the implementation of just one classification approach. Three atmospheric adjustments and five topographic corrections were examined using the greatest likelihood classification. In other studies, various methods were employed to classify land cover. For instance, while Noi and Kappas (2017) used RF, SVM, and K-nearest neighbour to classify six distinct land use/cover classes, Abdi (2020) used SVM, RF, and Extreme gradient boosting (XGB) to classify eight different classes (K-NN). Castro Gomez (2017) investigated the classification of the Sentinel-1 and Sentinel-2 datasets using machine learning.

Copyright © 2022 Nigerian Meteorological Society

The major goal of this research was to use machine learning techniques to assess how various atmospheric correction models influenced classification accuracy. The objective of this study was to test the precision of three atmospheric correction algorithms' estimations of land use and land cover.

Materials and Methods

The Okitipupa Local Government Area is the focus of this research (LGA). Okitipupa LGA is one of Ondo State's eighteen local government areas. Within Nigeria's Tropical rainforest zone, it is located between 6°25' and 6°30' N and 4°35' and 4°48' E. (Figure 1). At the 2006 census, it had an area of 803 km2 and a population of 233,565 people (Tobore *et al.*, 2019). The region is separated into two geological formations: Precambrian Basement Complex Granitic Rocks make up the northern half, while recent to tertiary sandy deposits make up the centre and southern halves (Tobore et al., 2019). The average annual temperature is 27.0°C, and the average annual precipitation is 1900 mm, with total annual rainfall frequently exceeding 2000mm.

Material and Methods

This research can be divided into five phases: (1) study area and satellite data, (2) application of atmospheric correction, (3) spectral indices, (4) land cover classification methods, and (5) accuracy assessment. The remote sensing image utilized in this study was acquired on the 5th of November 2021 (path/roll 190/055) from Explorer's official website (https://earthexplorer.usgs.gov/). The Landsat 8 ETM image was projected to the World Geographic System (WGS) 84 datum with the coordinate system of WGS_1984_UTM_Zone_31N. This image has a pixel size of 30 meters and eleven bands. Though not all the bands were utilized in this study, Table 1 gives an overview of the entire bands that make up the Landsat 8 (OLI/TIR) image.

Copyright © 2022 Nigerian Meteorological Society

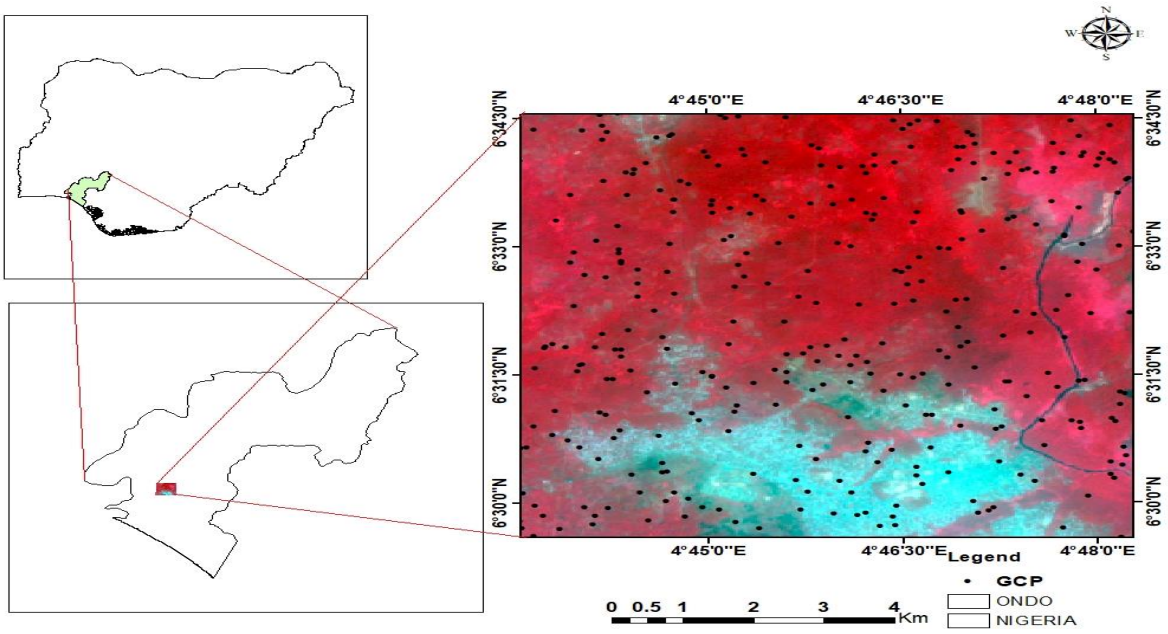

Figure1**:** Map of the study area in Okitipupa LGA, Ondo State, Nigeria.

Table 1. **Landsat 8 (OLI) bands and their respective wavelength in micrometres**

Band	Name	Wavelength (µm)	Resolution(m)
Band 1	Coastal/Aerosol	0.43-0.45	30
Band 2	Blue	0.45–0.51	30
Band 3	Green	0.53–0.59	30
Band 4	Red	0.64–0.67	30
Band 5	NIR	0.85–0.88	30
Band 6	SWIR1	1.57–1.65	30
Band 7	SWIR2	2.11–2.29	30
Band 8	Panchromatic	0.50-0.68	15
Band 9	Cirrus	1.36-1.38	30
Band 10	Thermal infrared (TIR) 1	10.6-11.19	100
Band 11	Thermal infrared (TIR) 2	11.50-12.51	100

Copyright © 2022 Nigerian Meteorological Society

Atmospheric Correction Methods

The correction methods are used to eliminate the noise in the satellite images. Though scientific literature is replete with so many correction methods, this study is focusing on: Fast Line-of-sight Atmospheric Analysis of Spectral Hypercubes (FLAASH), Quick Atmospheric Correction (QUAC), and Dark Object Subtraction (DOS). It is designed to eliminate the atmospheric effects caused by the molecular dispersion of particles in the atmosphere. It is determined by Equation (1).

$$L_{TOA} = \left(\frac{A\rho_{SUP}}{1-\rho_e S}\right)\left(\frac{B\rho_e}{1-\rho_e S}\right) + L_o \quad (1)$$

Where;
L_{TOA} is the spectral radiance reached by the satellite,
ρ_{SUP} is the reflectance of the pixel surface,
ρ_e is the reflectance of the average surface of the pixel of the surrounding region,
S is the spherical albedo of the atmosphere,
Lo is the radiance backscattered by the atmosphere,
A as well as B are coefficients that depend on the atmosphere and geometric conditions.

The first term of the equation corresponds to the reflectance of the surface that travels directly into the sensor while the second term corresponds to the luminosity of the surface that is dispersed by the environment. The distinction between ρ_{SUP} and ρ_e explains the "adjacency effect" (spatial blending of radiation between nearby pixels) caused by the atmospheric dispersion. The values of A, B, S, and Lo can be determined empirically from the MODTRAN4 standards. The vision and the solar angles of the measurement and the nominal values for the surface elevation, aerosol shape, and visible range of the scene must be specified (Marcello et al., 2016). This correction method was carried out with the FLAASH module of the software ENVI (v.5.1).

QUAC is an atmospheric correction method for visible band, NIR, and SWIR hyperspectral and multispectral data. Because this methodology was based on the values of light that penetrated the picture, QUAC's founding principles deviated from the standard atmospheric correction method. QUAC was characterized as a recording-based empirical technique. Without any further information, this specified type of parameter can be obtained directly from the atmosphere during the recording (Esthi and Bambang, 2016). The QUAC model was developed based on the experience of gathering average reflectance from a variety of content, including the spectrum of each section, where n denoted the amount of spectrum detected with shadows or a cloud-free basic scene. This means that the adjustment will be completed more quickly. The sun's

Copyright © 2022 Nigerian Meteorological Society

elevation angle and centre wavelength were also used by QUAC. Corrections could still be made using this method within the acceptable range of accuracy if the sensor did not have accurate radiation or wavelength, or if the intensity of sunlight was unknown. It's a dark targets-based algorithm. Because QUAC does not require first-principles radiative-transfer computations and simply requires an equation, the atmospheric correction approach is substantially faster than radiative transfer model-based methods. This correction method was carried out with the QUAC algorithm of the software ENVI (v.5.1).

Dark Object Subtraction (DOS) is an atmospheric correction system based on images. Due to air scattering, only a few pixels' radiances obscured by cloud pictures may be acknowledged by the satellite, according to Chavez (1996). The DOS method is based on the properties of the image. This correction method is the most widely used for the detection of land-use changes. Elements such as water, forests, and shadows are considered dark objects when their values of reflectance are close to zero. Dark objects are detected automatically when the pixel reflectance value is less than or equal to 1.0%. The assumption is that some pixels within the image receive 0% of the solar radiation (100% of shade), mainly due to the effect of topography, and the value of radiances corresponding to these pixels registered by the satellite corresponds to atmospheric dispersion (Chavez, 1988). If a dark object is found in the image, the minimum reflectance value in the histogram is assigned to such an object. From this minimum, it is possible to correct the entire scene by the effects of the atmospheric dispersion (Paolini et al., 2006; Cui et al., 2014). Surface reflectance was obtained using Equation (2)

$$P_{SUP} = \frac{d^2\pi(L_{TOA}-L_o)}{E_{TOA}cos_\theta} \quad (2)$$

Where;

d is the direct distance to the sun,

L_{TOA} is the spectral radiance to the satellite,

L_o is the backscatter glow through the atmosphere,

E_{TOA} is the solar spectral radiance on a surface perpendicular to the sun's rays outside the atmosphere, and

θ is the solar zenith angle.

This radiometric correction was carried out using the Semi-Automatic Classification plugin developed by Congedo (2013) in the QGIS (v.3.8).

Land Cover Classification Methods

This study is subjected to a supervised classification method using both Random

Copyright © 2022 Nigerian Meteorological Society

Forest (RF) and Support Vector Machine (SVM) classification algorithms. Random Forest (RF) classifier is a machine learning algorithm that combines many tree classifiers. To classify an input image, each tree classifier generates a unit vote for the most common class in the tree (Breiman 1999). RF, which is one of the most applied machines learning algorithms in classification studies (Basu et al., 2021; Berhane et al., 2018; Avcı et al 2022) increases the accuracy of the classification by creating more than one decision tree (Dubeau et al., 2017). RF classifier is capable of handling high data dimensionality and multi-linearity while still being fast and resistant to overfitting (Jagannath, 2020). The number of active variables in the random subset at each node and the number of trees in the forest are two parameters of RF. Several studies in the realm of remote-sensing applications have recently revealed that LULC classification utilizing RF has a reasonable performance (Adam *et al.,* 2014; Ma et al., 2017; Camargo et al., 2019).

SVM on the other hand is a supervised non-parametric statistical learning method. In this algorithm, no assumptions about the underlying data distribution are made (Vapnik, 1998). SVM is popular in remote sensing classification studies (Qian, et al., 2015) and it is stated that SVM can handle the classification of complex LULC (Pretorius et al., 2016). The main benefit of SVM is that it does not necessitate a large number of training samples to obtain reliable statistical features for each class (Chinsu, et al., 2015). A hyperplane can be formed with just a few critical training examples. The hyperplane will be used to further classify all of the testing samples. This might be accomplished by separating their bounds in feature space and categorizing each sample according to which side they fall on. (Petropoulos *et al*., 2012). The thematic classes of interest in this study are built-up, shrubs, vegetation and wetland/rivers. This is based on modified classification schemes by Anderson (1971) and Anderson et al., (1972).

Accuracy Assessment

To assess the accuracy, 500 randomly sampled ground control points (GCP) were generated. A Google Earth image of almost the same date as the Landsat image was used as a reference image. This GCP were used to generate error matrixes, also known as confusion matrixes by comparing the reference data, to the classification results. The accuracy of the results is the determining factor in judging whether this exercise is a success or not. The confusion matrix was calculated using the Compute

Copyright © 2022 Nigerian Meteorological Society

Confusion Matrix algorithm in Spatial Analyst Tools (ArcGIS 10.8).

RESULTS AND DISCUSSION

Visual characteristics of the atmospherically corrected images

The spectral signatures of three atmospherically adjusted Landsat 8 images of 2021 were examined after atmospheric adjustment. Using the mean value of all training and validation pixels for each class, the analysis was performed on four separate land cover classes: built-up, shrubs, vegetation, and wetland/rivers.

The image's visual quality was improved through a higher contrast ratio, indicating that the atmospheric adjustment was effective. The FLAASH image had the highest contrast ratio when the outcomes of atmospheric correction were visually contrasted (Figures 2-4). The normalized mean reflectance of some selected bands extracted from the three atmospheric correction models was revealed through band statistics (Figure 5). It was discovered that when compared to other models, the QUAC model had the highest mean values.

In comparison to the others, the values adjusted by the QUAC model were dramatically displaced, particularly in the RED band of the Landsat 8 image. In contrast to those from the top of the atmosphere (TOA) photos, each atmospheric correction method boosted the NDVI values. This demonstrated that when compared to other atmospheric correction approaches, the QUAC method produced higher NDVI values. This finding is consistent with Moravec et al., (2021) work on the "Effect of Atmospheric Corrections on NDVI: Inter-comparability of Landsat 8, Sentinel-2, and UAV Sensors". Table 2 contains the three AC models' mean values.

Image classification using SVM and RF classifiers

To provide a reliable estimation of the environmental assessment using Landsat 8 OLI for the study area, two different machine learning classification techniques were used to classify the three atmospherically corrected Landsat 8 images. In this regard, image classification based on advanced mathematical and machine learning algorithms of SVM and RF was produced (Figures 6 and 11). The aim is to evaluate the variations in LULC in the classification of the three AC models. Four major thematic classes were identified in the image i.e., the build-up, shrubs, vegetation, and water/rivers. Out of 11711 ha in the study area, the RF algorithm classified 1172 ha as a build-up area on the DOS image, 1172 ha on the QUAC image and 1040 ha on the FLAASH image (Table 3). Shrubs recorded 2688 ha (DOS), 2690

Copyright © 2022 Nigerian Meteorological Society

ha (QUAC) and 2851ha (FLAASH) respectively. The vegetation thematic class had 7546 ha (DOS), 7544 ha (QUAC) and 7665 ha (FLAASH). Wetland/rivers class had the least area extent by way of classification with 305 ha (DOS), 305 ha (QUAC) and 115 ha (FLAASH).

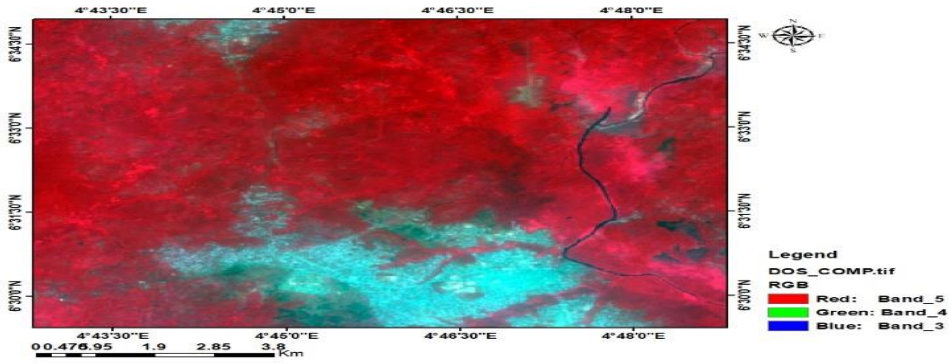

Figure 2: A composite RGB image of an atmospherically corrected image using the DOS algorithm

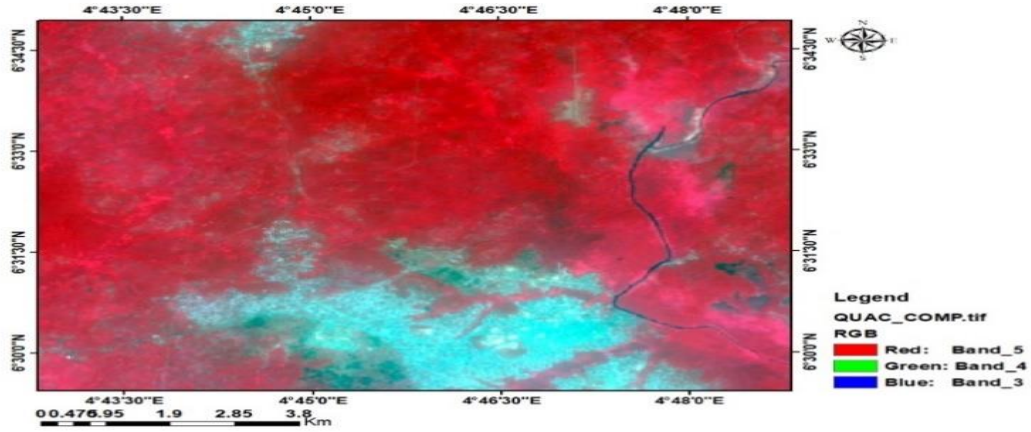

Figure 3: A composite RGB image of an atmospherically corrected image using the QUAC algorithm

Copyright © 2022 Nigerian Meteorological Society

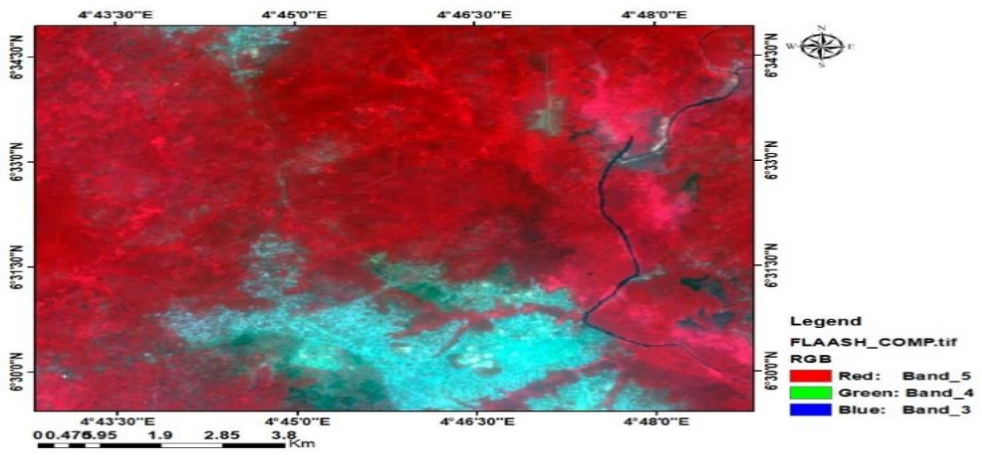

Figure 4: A composite RGB image of an atmospherically corrected image using the FLAASH algorithm

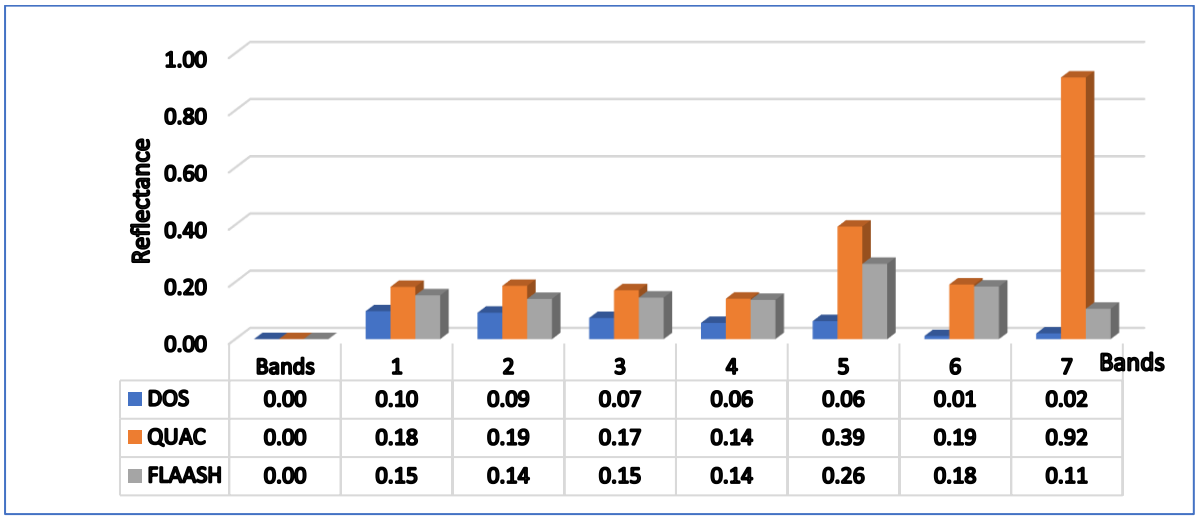

Figure 5: Band statistics of the normalized atmospherically corrected images using DOS, QUAC and FLAASH

Table 2: Normalized Difference Vegetation Index (NDVI) horizontal profile statistics of the atmospheric correction models

NDVI STATISTICS				
ALGORITHM	MIN	MAX	MEAN	StdDEV
FLAASH	0.13	0.45	0.34	0.05
QUAC	0.12	0.61	0.47	0.09
DOS	-0.12	0.15	0.05	0.05

Copyright © 2022 Nigerian Meteorological Society

Image classification using SVM and RF classifiers

To provide a reliable estimation of the environmental assessment using Landsat 8 OLI for the study area, two different machine learning classification techniques were used to classify the three atmospherically corrected Landsat 8 images. In this regard, image classification based on advanced mathematical and machine learning algorithms of SVM and RF was produced (Figures 6 and 11). The aim is to evaluate the variations in LULC in the classification of the three AC models. Four major thematic classes were identified in the image i.e., the build-up, shrubs, vegetation, and water/rivers. Out of 11711 ha in the study area, the RF algorithm classified 1172 ha as a build-up area on the DOS image, 1172 ha on the QUAC image and 1040 ha on the FLAASH image (Table 3). Shrubs recorded 2688 ha (DOS), 2690 ha (QUAC) and 2851ha (FLAASH) respectively. The vegetation thematic class had 7546 ha (DOS), 7544 ha (QUAC) and 7665 ha (FLAASH). Wetland/rivers class had the least area extent by way of classification with 305 ha (DOS), 305 ha (QUAC) and 115 ha (FLAASH).

Two distinct machine learning classification approaches were employed to classify the three atmospherically corrected Landsat 8 pictures to offer a valid estimate of the environmental assessment using Landsat 8 OLI for the research area. Image classification based on modern mathematical and machine learning methods of SVM and RF was developed in this regard (Figures 5 and 6). The overall goal is to assess the differences in LULC across the three AC models in terms of classification. The image contains four key subject classes: the build-up, bushes, greenery, and water/rivers. The RF algorithm classified 1172 ha of the 11711ha study area as a build-up region on the DOS picture, 1172 ha on the QUAC image, and 1040 ha on the FLAASH image (Table 3).

The built-up area was 1038 ha (DOS), 1100 ha (QUAC), and 1103 ha (DOS) according to the LULC statistics calculated using the SVM classifier across the three atmospherically adjusted pictures (FLAASH). Shrubs had a total area of 2086 ha (DOS), 1953 ha (QUAC), and 1982 ha (QUAC) (FLAASH). 8438 ha (DOS), 8416 ha (QUAC), 8559 ha (FLAASH), 147 ha (DOS), 243 ha (QUAC), and 67 ha (FLAASH) were registered for vegetation and wetland, respectively (Table 3).

Copyright © 2022 Nigerian Meteorological Society

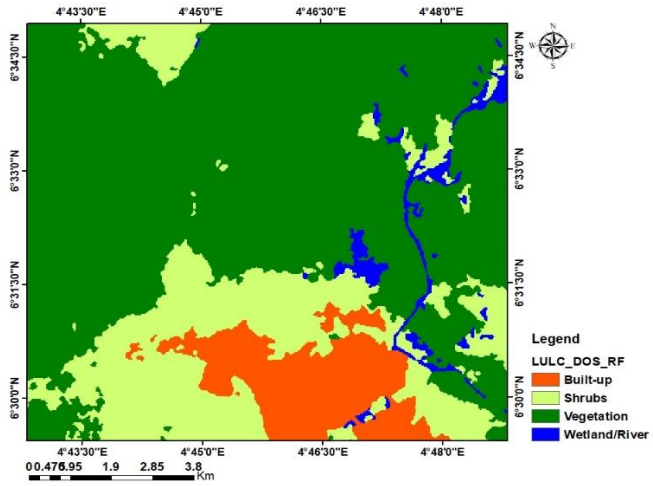

Figure 6: Land cover map using the Random Forests (RF) classification algorithm on DOS corrected image.

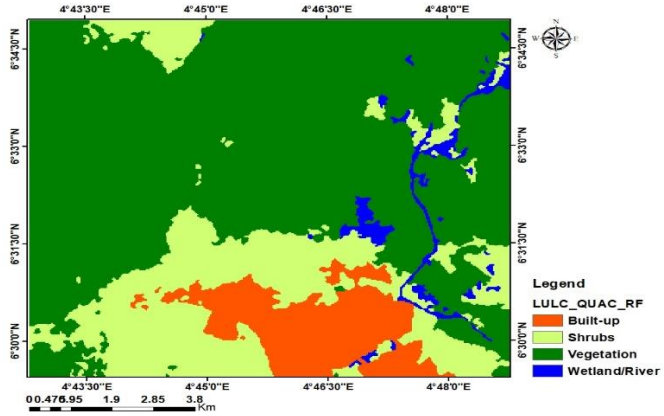

Figure 7: Land cover map using the Random Forests (RF) classification algorithm on QUAC corrected image.

Copyright © 2022 Nigerian Meteorological Society

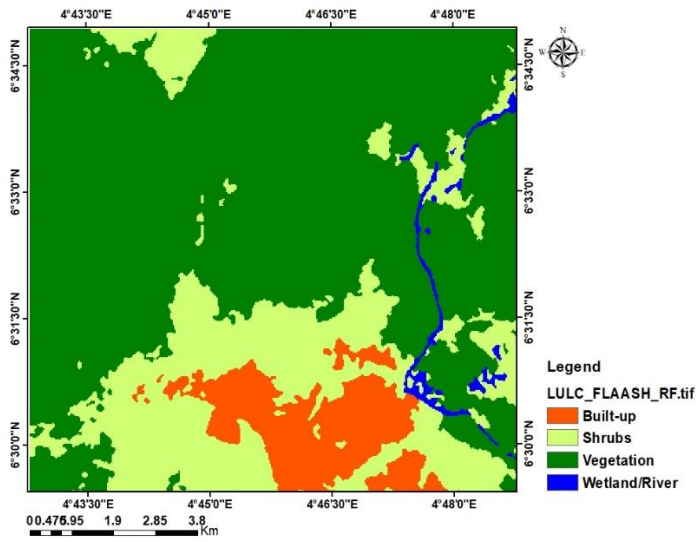

Figure 8: Land cover map using the Random Forests (RF) classification algorithm on FLAASH corrected image.

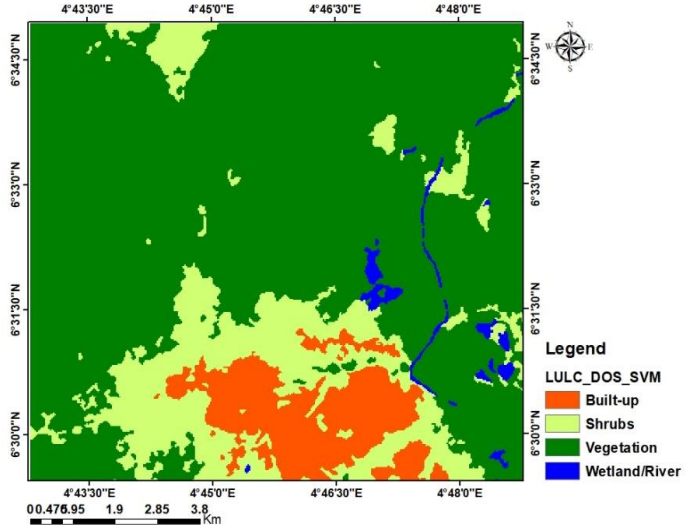

Figure 9: Land cover map using the Support Vector Machine (SVM) classification algorithm on DOS corrected image

Copyright © 2022 Nigerian Meteorological Society

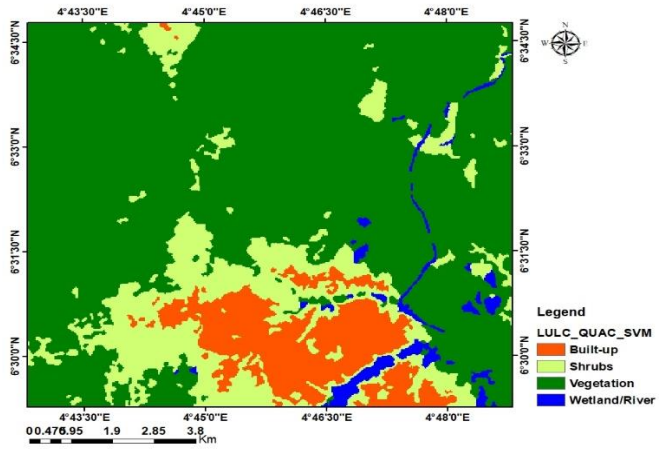

Figure 10: Land cover map using the Support Vector Machine (SVM) classification algorithm on QUAC corrected image

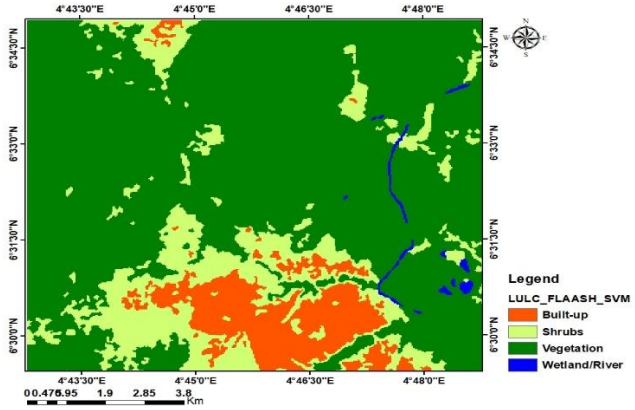

Figure 11: Land cover map using the Support Vector Machine (SVM) classification algorithm on FLAASH corrected image

Copyright © 2022 Nigerian Meteorological Society

Table 3: Land cover statistics derived from the three machine learning algorithms

	Random Forest (RF)						Support Vector Machine (SVM)					
	DOS		QUAC		FLAASH		DOS		QUAC		FLAASH	
LULC	Area (ha)	%	Area (ha)	%	Area (ha)	%	Area (ha)	%	Area (ha)	%	Area (ha)	%
Built-up	1172	10	1172	10	1040	9	1038	9	1100	9	1103	9
Shrubs	2688	23	2690	23	2851	24	2089	18	1953	17	1982	17
Vegetation	7546	64	7544	64	7665	65	8438	72	8415	72	8559	73
Wetland/River	305	3	305	3	155	1	146	1	243	2	67	1

Accuracy assessment of the classifiers based on the atmospheric correction model

The accuracy of classification was impacted by techniques, approaches, time and space. (Maxwell et al., 2018; Noi and Kappas, 2018; Rodriguez-Galiano and Chica-Rivas, 2018; Camargo et al., 2019). Several studies found slight to moderate differences in Land cover classification accuracy when different classifiers were used (Rwanga and Ndambuki, 2017, Leyk et al., 2018, Islam et al., 2018). A Land cover classification's accuracy varies not just by the classifier, but also by space and time. This could be due to differences in the atmosphere, surface, and lighting (Li et al., 2016). With the help of a confusion matrix, (Tables 4 - 9) the accuracy assessment of the LULC classifications was obtained. The findings revealed that the SVM_FLAASH has the highest overall accuracy (0.98) and kappa coefficient (0.96).

Tables 4-9 show that SVM has the highest accuracy performance among the three AC models, while RF has the lowest. This conclusion was consistent with Noi and Kappas's (2017) findings, with SVM having a higher accuracy output than RF. For example, Somdatta *et al.* (2011) used Hyperion data to test both FLAASH and QUACC methodologies and found that FLAASH performed better than QUAC in terms of atmospheric correction. Guo et al. (2012) discovered that FLAASH was more effective at reducing noise than QUAC

Copyright © 2022 Nigerian Meteorological Society

when they looked at spot data using both approaches. In contrast, when compared to FLAASH and QUAC models, Nazeer et al (2014) found that DOS had the most appropriate and consistent values. The variation in machine learning algorithms could be due to a variety of factors.

CONCLUSIONS

The remote sensing image utilized in this study was Landsat 8 OLI covering Okitipupa Local Government Area, on the 5th November 2021, downloaded from Earth Explorer (https://earthexplorer.usgs.gov/). Landsat 8 image was used to test the effects of applying three different atmospheric correction methods on land cover classification using Random Forest and SVM algorithms. This study showed that SVM is the best machine learning classifier for land cover/use classification and outperformed RF. This research concluded that the selection of classifiers is as important as the selection of the atmospheric correction method deployed during satellite image analysis. The accuracy assessment showed that SVM_FLAASH has the highest accuracy performance among the three AC models

Table 4 – Error matrix of the SVM_FLAASH classification

	Built-up	Shrubs	Vegetation	Wetland/Rivers	Total	U_Accuracy	Kappa
Built-up	48	0	1	0	49	0.98	
Shrubs	2	115	3	0	120	0.96	
Vegetation	0	0	317	1	318	1	
Wetland/Rivers	0	0	1	12	13	0.92	
Total	50	115	322	13	500	0	
P-Accuracy	0.96	1	0.98	0.92	0	0.98	
Kappa							0.96
O-Accuracy							0.98

Copyright © 2022 Nigerian Meteorological Society

Table 5: Error matrix of the SVM_QUAC classification

	Built-up	Shrubs	Vegetation	Wetland/Rivers	Total	U-Accuracy	Kappa
Built-up	48	1	1	0	50	0.96	
Shrubs	2	114	4	0	120	0.95	
Vegetation	0	0	316	2	318	0.99	
Wetland/Rivers	0	0	1	11	12	0.91	
Total	50	115	322	13	500	0	
P-Accuracy	0.96	0.99	0.98	0.85	0	0.98	
Kappa Coeff.							0.95
O-Accuracy							0.97

Table 6: Error matrix of the SVM_DOS classification

	Built-up	Shrubs	Vegetation	Wetland/Rivers	Total	U-Accuracy	Kappa
Built-up	47	2	2	0	51	0.92	
Shrubs	3	112	4	0	119	0.94	
Vegetation	0	1	314	2	317	0.99	
Wetland/Rivers	0	0	2	11	13	0.85	
Total	50	115	322	13	500	0	
P-Accuracy	0.94	0.97	0.98	0.85	0	0.97	
Kappa Coeff.							0.93
O-Accuracy							0.96

Copyright © 2022 Nigerian Meteorological Society

Table 7: Error matrix of the RF_FLAASH classification

	Built-up	Shrubs	Vegetation	Wetland/Rivers	Total	U-Accuracy	Kappa
Built-up	48	3	0	0	51	0.94	
Shrubs	2	96	0	0	98	0.98	
Vegetation	0	16	322	0	338	0.95	
Wetland/Rivers	0	0	0	13	13	1	
Total	50	115	322	13	500	0	
P-Accuracy	0.96	0.83	1	1	0	0.95	
Kappa							0.92
O-Accuracy							0.96

Table 8: Error matrix of the RF_QUAC classification

	Built-up	Shrubs	Vegetation	Wetland/Rivers	Total	U-Accuracy	Kappa
Built-up	47	3	0	0	50	0.94	
Shrubs	3	90	0	0	93	0.96	
Vegetation	0	22	322	0	344	0.93	
Wetland/Rivers	0	0	0	13	13	1	
Total	50	115	322	13	500	0	
P-Accuracy	0.94	0.78	1	1	0	0.94	
Kappa							0.88
O-Accuracy							0.94

Copyright © 2022 Nigerian Meteorological Society

Table 9: Error matrix of the RF_DOS classification

	Built-up	Shrubs	Vegetation	Wetland/Rivers	Total	U_Accuracy	Kappa
Built-up	44	4	0	0	49	0.92	
Shrubs	5	85	0	0	90	0.94	
Vegetation	0	26	322	1	349	0.92	
Wetland/Rivers	0	0	0	12	12	1	
Total	50	115	322	13	500	0	
P-Accuracy	0.90	0.74	1	0.92	0	0.928	
Kappa							0.85
O-Accuracy							0.72

ACKNOWLEDGMENTS

The authors appreciate the contributions of Industrial Training students and Youth Corp members attached to the Department of Environmental Management and Biometrics, Forestry Research Institute of Nigeria (FRIN) during the data acquisition phase of this work.

REFERENCES

Abdi, A.M. (2020). Land cover and land use classification performance of machine learning algorithms in a boreal landscape using Sentinel-2 data. *GIScience Remote Sens.* 57: 1–20.

Adam, E., Mutanga, O., Odindi, J. and Abdel-Rahman, E.M. (2014). Land-use/cover classification in a heterogeneous using coastal landscape Rapid Eye imagery: Evaluating the performance of random forest and support vector machines classifiers. *Int. J. Remote Sens.* 35, 3440–3458.

Agrawal, G., Sarup, J., Bhopal, M (2011). Comparison of QUAC and FLAASH atmospheric correction modules on EO-1 Hyperion data of Sanchi. *Int. J. Adv. Eng. Sci. Technol*., 4, 178–186.

Anderson, James R. (1971), Land use classification schemes used in selected recent geographic applications of remote sensing: *Photogramm. Eng.,* 37 (4), 379-387.

Anderson, James R., Hardy, Ernest E., and Roach, John T., (1972), A land-use classification system for use with remote-sensor data: *U.S. Geol. Survey Cire.* 671.

Avcı, C. Budak, M. Yagmur, N., & Balcık, F. B. (2022). Comparison between random forest and support vector machine algorithms for LULC classification. International Journal

Copyright © 2022 Nigerian Meteorological Society

of Engineering and Geosciences, 8(1), 01-10

Ballanti, L., Blesius, L., Hines, E. and Kruse, B. (2016). Tree species classification using hyperspectral imagery: A comparison of two classifiers. *Remote Sens.* 8: 445.

Basu, T., Das, A., Pham, Q. B., Al-Ansari, N., Linh, N. T. T., & Lagerwall, G. (2021). Development of an integrated peri-urban wetland degradation assessment approach for the Chatra Wetland in eastern India. Scientific reports, 11(1), 1-22.

Berhane, T. M, Lane, C. R., Wu, Q, Autrey, B. C., Anenkhonov, O. A., Chepinoga, V. V., Liu, H. (2018). Decision-tree, rule-based, and random forest classification of high-resolution multispectral imagery for wetland mapping and inventory. *Remote sensing*, 10(4), 580.

Breiman, L. (1999). Random forests. UC Berkeley TR567.

Callieco, F.; Dell'Acqua, F (2011). A comparison between two radiative transfer models for atmospheric correction over a wide range of wavelengths. *Int. J. Remote Sens.*, 32, 1357–1370.

Camargo, F.F., Sano, E.E., Almeida, C.M., Mura, J.C. and Almeida, T. A. (2019). Comparative assessment of machine-learning techniques for land use and land cover classification of the Brazilian tropical savanna using ALOS-2/PALSAR-2 polarimetric images. *Remote Sens.*11, 1600.

Castro Gomez, M.G. (2017). Joint use of Sentinel-1 and Sentinel-2 for land cover classification: A machine learning approach. *Lund Univ. GEM thesis Ser.* NGEM01: 20162

Chavez PS. (1996). Image-based atmospheric corrections-revisited and improved. *Photogrammetric engineering and remote sensing* 62 (9), 1025-1036.

Chavez, P.S., Jr. (1988) An improved dark-object subtraction technique for atmospheric scattering correction of multispectral data. *Remote Sens. Environ.*, 24, 459–479.

Chinsu Lin., Chao-Cheng Wu, Khongor Tsogt, Yen-Chieh Ouyang and Chein-I Chang. (2015) Effects of atmospheric correction and pan-sharpening on LULC classification accuracy using WorldView-2 imagery. *INFORMATION PROCESSING IN AGRICULTURE* 2: 25–36.

Chrysoulakis N., Abrams M., Feidas H. and Arai K. (2010). Comparison of atmospheric correction methods using ASTER data for the area of Crete, Greece. *Int. J. Remote Sens.* 31: 6347–6385.

Claverie M., Ju J., Masek J.G., Dungan J.L., Vermote E.F., Roger J.C., Skakun S.V. and Justice C. (2018). The Harmonized Landsat and Sentinel-2 surface reflectance data set. *Remote Sens. Environ.* 219:145–161.

Cohen, W.B.; Goward, S.N (2004). Landsat's role in ecological applications of remote sensing. *BioScience*, 54, 535–545.

Congedo, L (2013). Semi-Automatic Classification Plugin for QGIS; Technical Report; Sapienza University, ACC Dar Project: Rome, Italy,.

Copyright © 2022 Nigerian Meteorological Society

Cui, Q.Y.; Gaillard, M.J.; Lemdahl, G.; Stenberg, L.; Sugita, S.; Zernova, G (2014). Historical land-use and landscape change in Southern Sweden and implications for present and future biodiversity. Ecol. Evol., 4, 3555–3570.

Dubeau, P., King, D. J., Unbushe, D. G., & Rebelo, L. M. (2017). Mapping the Dabus wetlands, Ethiopia, using random forest classification of Landsat, PALSAR and topographic data. Remote Sensing, 9(10), 1056.

El Hajj, M.; Bégué, A.; Lafrance, B.; Hagolle, O.; Dedieu, G.; Rumeau, M (2008). Relative radiometric normalization and atmospheric correction of a SPOT 5 time series. *Sensors*, 8, 2774–2791.

Esthi Kurnia Dewi and Bambang Trisakti (2016). Comparing Atmospheric Correction Methods for Landsat 8 (OLI) Data. *International Journal of Remote Sensing and Earth Science* 13(2), 235-243

Fan, J.W.; Zhong, H.P.; Harris, W.; Yu, G.R.; Wang, S.Q.; Hu, Z.M.; Yue, Y.Z (2007). Carbon storage in the grassland of China based on field measurement of above- and below-ground biomass. *Clim. Chang.*, 86, 375–396.

Guo Y., Zeng F., (2012), Atmospheric Correction Comparison of Spot-5 Image Based on Model Flaash and Model Quac. International Archives of the Photogrammetry, *Remote Sensing and Spatial Information Sciences*, XXXIX-B7: 7-11

Hansen, M.C.; Loveland, T.R (2012). A review of large area monitoring of land cover change using Landsat data. *Remote Sens. Environ.*, 122, 66–74

He, C.; Zhang, Q.; Li, Y.; Li, X.; Shi, P (2005). Zoning grassland protection area using remote sensing and cellular automata modeling-A case study in Xilingol steppe grassland in northern China. *J. Arid Environ.*, 63, 814–826.

Islam K., Jashimuddin M., Nath B. and Nath T.K. (2018). Land use classification and change detection by using multi-temporal remotely sensed imagery: The case of Chunati wildlife sanctuary, Bangladesh. *Egypt. J. Remote Sens. Space Sci.* 21: 37–47.

Jagannath, V. (2020). "Random Forest Template for TIBCO Spotfire® - Wiki Page TIBCO Community." https://community.tibco.com/wiki/random-forestemplate-tibco-spotfire

Janzen, T.D.; Fredeen, L.A.; Wheate, D.R (2006). Radiometric correction techniques and accuracy assessment for Landsat TM data in remote forested regions. Can. *J. Remote Sens.*, 32, 330–340

Kaufman Y.J., Wald A.E., Remer L.A., Gao B.-C., Li R.-R. and Flynn, L. (1997). The MODIS 2.1 μm channel—Correlation with visible reflectance for use in remote sensing of aerosol. *Geosci. Remote Sens.* 35: 1286–1298.

Koc-San D. (2013). Evaluation of different classification techniques for the detection of glass and plastic greenhouses from WorldView-2 satellite imagery. *J. Appl. Remote Sens*. 7: 073553.

Copyright © 2022 Nigerian Meteorological Society

Körner, I.; Oreopoulos, L.; Feingold, G.; Remer, L.A.; Altaratz, O (2008). How small is a small cloud? *Atmos. Chem. Phys.*, 8, 3855–3864.

Kruse, F.A (2004). Comparison of ATREM, ACORN, and FLAASH atmospheric corrections using low-altitude AVIRIS data of Boulder, CO. In Proceedings of the 13th JPL Airborne Geoscience Workshop, Pasadena, CA, USA.

Lantzanakis G., Mitraka Z. and Chrysoulakis N. (2016). Comparison of physically and image-based atmospheric correction methods for Sentinel-2 satellite imagery. In Proceedings of the Fourth International Conference on Remote Sensing and Geoinformation of the Environment (RSCy2016), Paphos, Cyprus, 9688: 96880.

Leyk S., Uhl J.H., Balk D. and Jones B. (2018). Assessing the accuracy of multi-temporal built-up land layers across rural-urban trajectories in the United States. *Remote Sens. Environ.*, 204: 898–917.

Li X., Chen W., Cheng X. and Wang L. (2016). A comparison of machine learning algorithms for mapping complex surface-mined and agricultural landscapes using ZiYuan-3 stereo satellite imagery. *Remote Sens.* 8: 514.

Lin C., Wu C.C., Tsogt K., Ouyang Y.C. and Chang C.I. (2015). Effects of atmospheric correction and pansharpening on LULC classification accuracy using WorldView-2 imagery. *Inf. Process. Agric.* 2: 25–36.

López-Serrano, P.M.; Corral-Rivas, J.J.; Díaz-Varela, R.A.; Álvarez-González, J.G.; López-Sánchez, C.A (2016). Evaluation of radiometric and atmospheric correction algorithms for aboveground forest biomass estimation using Landsat 5 TM data. Remote Sens., 8, 369

Ma L., Li M., Ma X., Cheng L., Du P. and Liu Y. (2017). A review of supervised object-based land-cover image classification. *J. Photogramm. Remote Sens.*130: 277–293.

Marcello, J.; Eugenio, F.; Perdomo, U.; Medina, A (2016). Assessment of atmospheric algorithms to retrieve vegetation in natural protected areas using multispectral high-resolution imagery. *Sensors*, 16, 1624.

Martins, V.S.; Barbosa, C.C.F.; de Carvalho, L.A.S.; Jorge, D.S.F.; Lobo, F.D.L.; Novo, E.M.L.D.M (2017). Assessment of atmospheric correction methods for Sentinel-2 MSI images applied to Amazon floodplain lakes. *Remote Sens.*, 9, 322

Maxwell A.E., Warner T.A. and Fang F. (2018). Implementation of machine-learning classification in remote sensing: An applied review. *Int. J. Remote Sens.* 39: 2784–2817.

Moravec D., Komárek J., López-Cuervo Medina S. and Molina I. (2021). Effect of Atmospheric Corrections on NDVI: Intercomparability of Landsat 8, Sentinel-2, and UAV Sensors. *Remote Sens.* 13: 3550.

Nazeer M., Nichol JE. and Yung Y. (2014). Evaluation of atmospheric correction models and Landsat surface reflectance product in an urban coastal environment.

Copyright © 2022 Nigerian Meteorological Society

International Journal of Remote Sensing 35(16): 6271 – 6291.

Noi P.T. and Kappas M. (2017). Comparison of random forest, k-nearest neighbour, and support vector machine classifiers for land cover classification using sentinel-2 imagery. *Sensors (Switzerland),* 18.

Paolini, L.; Grings, F.; Sobrino, J.A.; Jiménez Muñoz, J.C.; Karszenbaum, H (2006). Radiometric correction effects in Landsat multi-date/multi-sensor change detection studies. *Int. J. Remote Sens.*, 27, 685–704.

Petropoulos G.P., Kalaitzidis C. and Prasad Vadrevu K. (2012). Support vector machines and object-based classification for obtaining land-use/cover cartography from Hyperion hyperspectral imagery. *Comput. Geosci.* 41: 99–107.

Pons, X.; Pesquer, L.; Cristóbal, J.; González-Guerrero, O (2014). Automatic and improved radiometric correction of Landsat imagery using reference values from MODIS surface reflectance images. *Int. J. Appl. Earth. Obs.,* 33, 243–254

Pretorius, L., Brown, L. R., Bredenkamp, G. J. & van Huyssteen, C. W. (2016). The ecology and classification of wetland vegetation in the Maputaland Coastal Plain, South Africa. Phytocoenologia, 46(2), 125-139.

Prieto-Amparán, J.A.; Pinedo-Alvarez, A.; Villarreal-Guerrero, F.; Pinedo-Alvarez, C.; Morales-Nieto, C.; Manjarrez-Domínguez, C (2016). Past and future spatial growth dynamics of Chihuahua city, Mexico: Pressures for land use. *Int. Geo-Inf.,* 5, 235

Qian, Y., Zhou, W., Yan, J., Li, W., & Han, L. (2015). Comparing machine learning classifiers for object-based land cover classification using very high-resolution imagery. *Remote Sensing,* 7(1), 153-168.

Rodriguez-Galiano V.F. and Chica-Rivas (2014). M. Evaluation of different machine learning methods for land cover mapping of a Mediterranean area using multi-seasonal Landsat images and Digital Terrain Models. *Int. J. Digit. Earth.* 7: 492–509.

Roy, D.P.; Zhang, H.K.; Ju, J.; Gomez-Dans, J.L.; Lewis, P.E.; Schaaf, C.B.; Sun, Q.; Li, J.; Hung, H.; Kovalskyy, V (2016). A general method to normalized Landsat reflectance data to nadir BRDF adjusted reflectance. *Remote Sens. Environ.*, 176, 255–271

Rumora L., Miler M., Medak, D. (2019). Contemporary comparative assessment of atmospheric correction influence on radiometric indices between Sentinel-2A and Landsat 8 imagery. *Geocarto Int*. 1–15.

Ruppert, J.C.; Linstädter, A (2014). Convergence between ANPP estimation methods in grasslands—A practical solution to the comparability dilemma. *Ecol. Indic.*, 36, 524–531.

Rwanga S.S. and Ndambuki J.M. (2017). Accuracy assessment of land use/land cover classification using

Copyright © 2022 Nigerian Meteorological Society

remote sensing and GIS. *Int. J. Geosci*. 8: 611.

Somdatta C. and Chakrabarti S., (2011). Preprocessing of Hyperspectral Data: A case study of Henry and Lothian Islands in Sunderban Region, West Bengal, India. *International Journal of Geomatics and Geosciences* 2(2).

Sonobe R., Yamaya Y., Tani H., Wang X., Kobayashi N. Mochizuki K. and Ichiro (2017). Assessing the suitability of data from Sentinel-1A and 2A for crop classification. *GIScience Remote Sens*. 54: 918–938.

Tan, K.C.; San Lim, H.; MatJafri, M.Z.; Abdullah, K (2012). A comparison of radiometric correction techniques in the evaluation of the relationship between LST and NDVI in Landsat imagery. Environ. Monit. Assess., 184, 3813–3829.

Tobore A, Oyerinde G, Senjobi B.A and Ogundiyi T.T (2019). Potentials and Characteristics of Landsat Imagery about Land Use /Cover in Okitipupa Metropolis, Ondo State, Nigeria. *Journal of Agricultural Science and Environment* 19(1 &2): 150-158

Vanonckelen S., Lhermitte S. and Van Rompaey A. (2013). The effect of atmospheric and topographic correction methods on land cover classification accuracy. *Int. J. Appl. Earth Obs. Geoinf.* 24: 9–21.

Vapnik, V. (1998). The support vector method of function estimation. In Nonlinear modelling (55- 85). Springer, Boston, MA.

Vázquez-Quintero, G.; Solís-Moreno, R.; Pompa-García, M.; Villarreal-Guerrero, F.; Pinedo-Alvarez, C.; Pinedo-Alvarez, A (2018). Detection and projection of forest changes by using the Markov Chain Model and Cellular Automata. Sustainability, 8, 236. *Remote Sens.* 10, 219 21 of 23 30.

Xie, Y.C.; Sha, Z.Y.; Yu, M.; Bai, Y.F.; Zhang, L (2009). A comparison of two models with Landsat data for estimating above-ground grassland biomass in Inner Mongolia, China. *Ecol. Model.*, 220, 1810–1818.

Zhao, P.; Dengsheng, L.; Guangxing, W.; Chuping, W.; Yujie, H.; Shuquan, Y (2016). Examining spectral reflectance saturation in Landsat imagery and corresponding solutions to improve forest aboveground biomass estimation. *Remote Sens.*, 8, 469.

Copyright Statement

Open Access article distributed under the terms of the Creative Commons License [CC BY-NC-SA 4.0] http://creativecommons.org/licenses/by-nc-sa/4.0 Condition of use: The license lets others remix, adapt, and build upon your work non-commercially, as long as they credit the authors and license their new creations under the identical terms.